Elimination of the Voltage Output Fluctuations of a Vienna Active Rectifier-I Integrated Under Unsymmetrical Faults Based Wind Power Plant

Inas M. O. Mohammed,[1]Michael Njoroge Gitau, [1]and Ramesh C. Bansal [2,1]

[1]Department of Electrical, Electronics and Computer Engineering, University of Pretoria, Pretoria, South Africa

[2]Department of Electrical Engineering, University of Sharjah, Sharjah, United Arab Emirates

*Address correspondence to Ramesh C. Bansal, Department of Electrical Engineering, University of Sharjah, Sharjah, United Arab Emirates. E-mail: rcbansal@ieee.org

Abstract

In this article, a fault ride-through controller is proposed with the use of proportional-integral compensator and electronic sensors for riding-through alternative current faults in a wind power plant collection grid connected with a permanent magnet synchronous generator. Three parallel-connected wind energy conversion units supplying a direct current (DC) load are simulated and discussed. It is found that the sub-module will directly adjust the transmission of power and protect the generator from overheating, which can occur due to voltage fluctuation. Furthermore, a DC voltage controller is designed to ensure a stable closed-loop system, and the system stability is verified using bode plots. The dynamic response of the system is demonstrated with the use of power simulator (PowerSim, Rockville, USA) software to verify the reliability of the proposed rectifier topology.

Keywords: voltage control; fault ride through; vienna active rectifier-I; wind power; transient stability; generation transients; fault clearance

1. Introduction

Direct current (DC) power transmission and distribution systems have received practical acceptance in power grids toward renewable energy resources. Moreover, DC systems offer more advantages over the alternative current (AC) systems such as [1–5]: (i) A synchronization procedure is more flexible than that on AC systems. (ii) The absence of reactive power enhances the general system efficiency. (iii) It is easy to integrate the renewable energy sources into a DC system with less complicated control strategies at low cost. (iv) The DC distribution systems have a high penetration level of compressed converters used to interface both distributed generators (DGs) and loads, yields a sustainable power load, unlike traditional AC distribution systems. In this regard, recent research studies have been developed further to improve DC technology. For an AC transmission system, each wind energy conversion unit (WECU) on a wind power plant (WPP) includes a big size 50- or 60 Hz power transformer [2–6]. In this work, the power transformers are replaced by the power electronic converters. The weight of a power transformer is extremely higher if compared to a power electronic converter of identical features. The classical full-bridge active rectifiers are the power electronic converter topology mostly used in studies being done to design the DC combination grids for WPPs [7, 8]. The classical active rectifier has a large number of controlled switches which operate at

1

a high switching frequency, then the efficiency of the wind farm is low because of the switching losses [2, 8–10]. Since the number of grid-connected wind farms is continuously increasing, the WPPs have to play a considerable role in maintaining grid stability, which requires that the wind turbine generator (WTG) on wind farm stay linked to the power grid during any fault conditions. The fault ride-through (FRT) is an expression used to explain the ability of a wind farm to contribute to the grid during faults, which is critical for assuring the power system stability [1–4]. A WPP generally consists of a large number of WTGs linked jointly at the main bus. The WECU are grouped into two categories [11, 12]

1. Fixed speed WECU: (e.g. squirrel cage induction generator (SCIG)),

2. Variable speed WECU: this type is grouped into two classes,

  i. permanent magnet synchronous generator (PMSG) based wind turbine (WT) with a full rating converter,

  ii. Doubly fed induction generator (DFIG) based WT with a fractional rating converter.

The full rating converters cutoff the synchronous machine speed from the grid frequency and supply adjustable operation over a wide range of speed [12]. The variable speed WTGs can monitor the power speedily and flexible with active power electronic converters.

One of the considerable challenges in wind energy conversion systems (WECSs) is to handle the discontinuity of the wind and to protect the grid stability. The power electronic converters and energy storage systems are substantial components to maintain the continuation of wind power. Conventional converters have the following demerits [13, 14].

1. Only a buck or a boost converter, that is, their attainable DC voltage output is higher or lower than the input AC voltage.

2. Susceptible to electromagnetic interference (EMI), which reduces system reliability.

When PMSG has been integrated with WT, the studies have shown that the PMSG has many advantages such as, (i) it can ride through several grid faults, (ii) able to have an instant disconnection from the grid in case of a fault and return fast into regular operation after the fault, and (iii) has the ability to smooth-out the discontinuous power fluctuation from the wind [15]. Vienna active rectifier-I, introduced initially by Kolar [16], is one of several types of converters that can be selected as a generator side converter for WECSs. The Vienna active rectifier-I has been chosen to be an efficient and cost-effective rectifier, and that recognizes the fundamentals of power quality and power reliability applications [2, 16]. Furthermore, it has many advantages over conventional and other types of active rectifiers, for example (i) has the capability of double boosting effect because it consists of two inductors on input and output sides, which can improve the rectifier features, (ii) it has the ability of buck-boost operation, (iii) allows transmission of the power to the DC-links even if the supply voltage is positive or negative, (iv) involvement of a single switch per power cell, and that permits to construct a highly stable and reliable rectifier, (v) it can obtain two DC-output voltages, (vi) the DC-ripples decrease for a given capacitor value, (vii) it has the possibility of continuous current modes, (viii) it has less number of active semiconductor devices, (ix) low current total harmonic

distortion (THD), and (x) high power density due to the three switches which are based on three-level configurations. Therefore, it has been applied in several high voltages and high power applications.

The main goal of this work is the development of a WECS-based DC transmission technology to improve the system stability and FRT capability of the WPP. The improvement is made by including an interface between a three-phase, three-unit variable speed AC synchronous generator and a constant DC-bus, based modular voltage source converter (VSC). For maintaining high power, as well as conserving a constant DC-bus voltage. The interface is desired to ensure high energy efficiency by maintaining a stable DC-bus voltage.

The DC collection grid in this article is built using a parallel connection of WPPs each consisted of PMSG and Vienna-I rectifier and connected to the load via a DC-link.

The rest of this work is organized as follows; section 2 presents the modeling and control of the Vienna active rectifier-I, including rectifier structure and analysis. The design of a DC-bus voltage controller is introduced in section 3 using bode plots for the compensator to evaluate the system stability. Section 4 discusses the fault effect elimination and analysis, as well as the overall simulated system is discussed in this section. Comprehensive simulations using PSIM software are shown in Section 5. The conclusion of this work is presented in section 6.

2. Modeling and Control of the Vienna Rectifier-I

2.1. Rectifier structure and modeling

The topology of a three-phase Vienna active rectifier-I has been designated as shown in Figure 1, [2, 17–25]. The topology contains three identical power electronic cells; each one is connected individually to a phase input. Each power cell involves one active switch and six diodes; the output of all the stages are connected to a middle link of output capacitors (which is used as power storage device and DC ripple reducer). The middle link of the capacitors is functionally connected to a neutral power by connecting the middle link of one arm of the diode bridges of all the three-phases. The control details of the studied rectifier have been described in refs. [16, 22–25]; the control of the three switches ensures the desired balanced output DC voltage. The rectifier is substantially a boost converter and has a three-level structure of output voltage, VC1 is one-half of the overall output voltage, (VC1 + VC2) has to be higher than the peak of the supply voltage Vs to ensure continuous conduction.
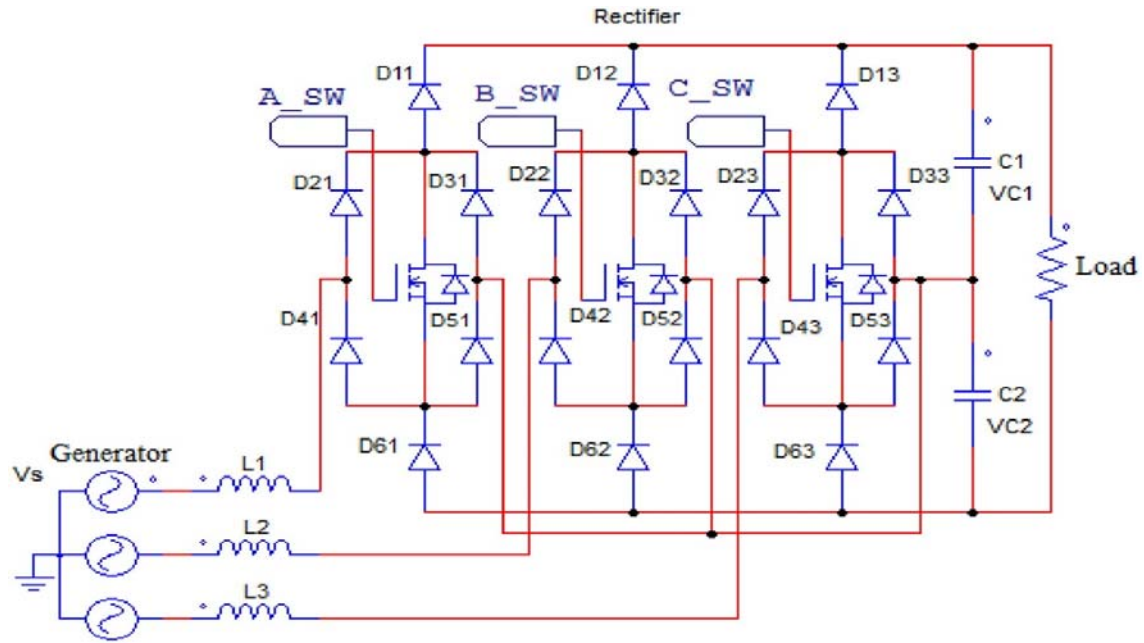
Figure 1. Three-phase Vienna rectifier-I topology.

The switching frequency of the rectifier is very high when compared with the supply frequency resulting in a lower value of the boost inductor. The generation side three-phase voltages can be represented as follows [16].

$$
\begin{aligned}
e_a &= E \sin (\omega_s\, t) \\
e_b &= E \sin (\omega_s\, t - 120) \\
e_c &= E \sin (\omega_s\, t + 120)
\end{aligned}
$$

(1)

where e_a, e_b, and e_c are the three-phase generation instant voltages, E is the maximum generator output voltage, ω_s is the generator angular velocity.

Equation (1) can be rewritten as follows.

$$
\begin{aligned}
e_a &= Ri_a + L\frac{di_a}{dt} + v_{an} \\
e_b &= Ri_b + L\frac{di_b}{dt} + v_{bn} \\
e_c &= Ri_c + L\frac{di_c}{dt} + v_{cn}
\end{aligned}
$$

(2)

where R is the internal generator resistance, L is the generator inductance, v_{an}, v_{bn}, and v_{cn} are the terminal voltages of the rectifier [2, 20–25].

2.2. Small-signal modeling of a Vienna rectifier-I

The analysis of the system response to small disturbances is called small-signal modeling of the system. The non-linear state-space equation describing the system operation can be represented as follows [26].

$$\dot{x} = Ax + Bu$$

(3)

where A is the system matrix, B is the input matrix, x is the state vector, and u is the input vector.

$$[v_d \ v_q \ v_0]^T = Z[v_a \ v_b \ v_c]^T$$

(4)

$$[i_d \ i_q \ i_0]^T = Z[i_a \ i_b \ i_c]^T$$

(5)

where Z is the *abc/dq*0 transformation matrix, i_d and i_q are the *d* and *q* axis currents, v_d and v_q are the *d* and *q* axis voltages, *d* is the duty cycle, v_o is the total DC output voltage; and can be represented as follows.

$$v_o = v_{o,u} + v_{o,l}$$

(6)

$$\Delta v_o = v_{o,u} - v_{o,l}$$

(7)

Δv_o is the variation between the two partial DC output buses, and should be equal to zero,

$$\begin{bmatrix} V_d \\ V_q \\ V_{s0} \end{bmatrix} = \begin{bmatrix} \sqrt{2}\,V_s \\ 0 \\ 0 \end{bmatrix}$$

(8)

$$\begin{bmatrix} I_d \\ I_q \\ I_0 \end{bmatrix} = \begin{bmatrix} \sqrt{2}\,I_s^* \\ 0 \\ 0 \end{bmatrix}$$

(9)

where V_s is the rms supply voltage, I_s and v_o are the reference values of the AC and total DC output voltage, respectively.
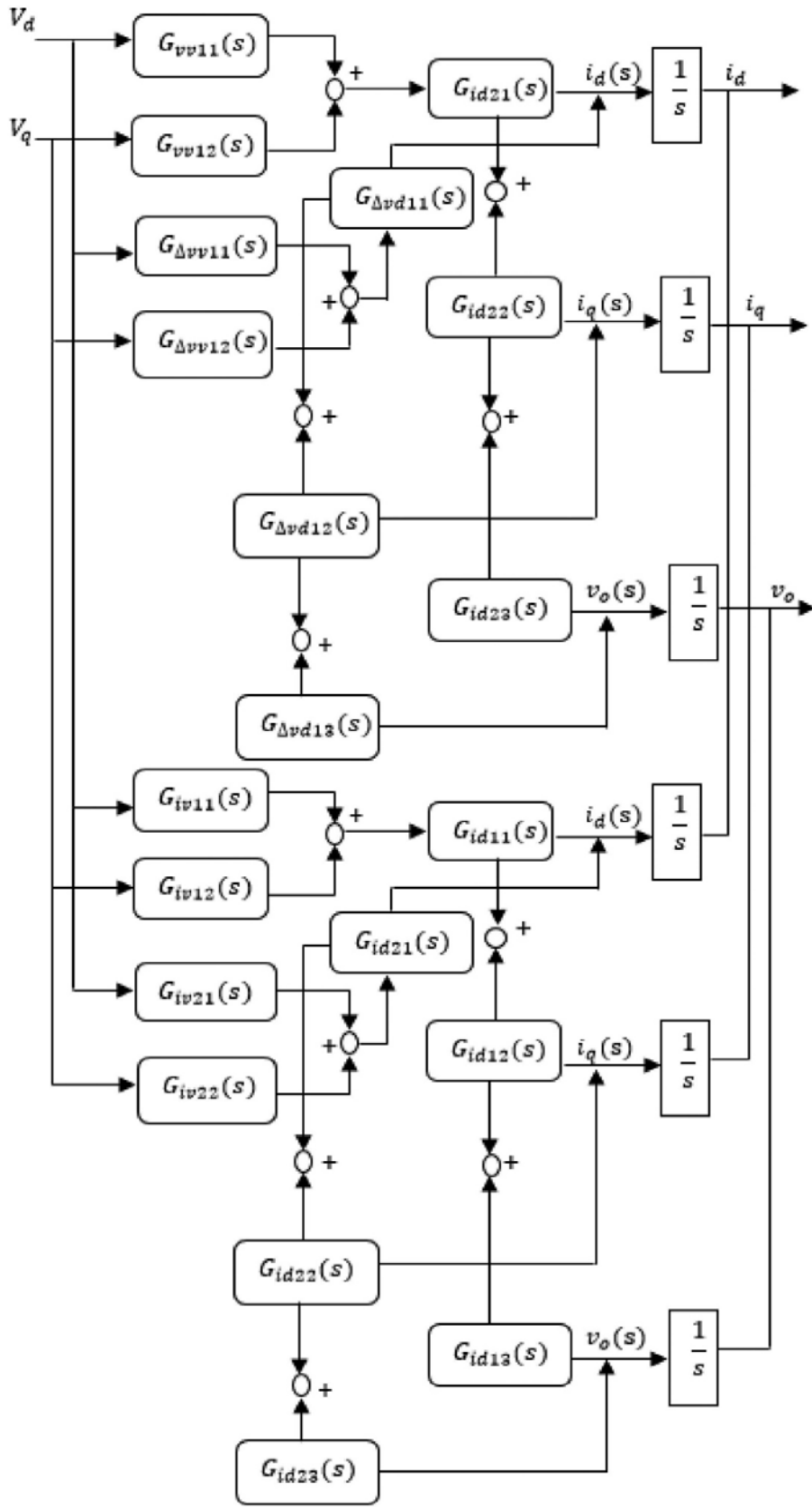
Figure 2. Transfer-function block diagram of the rectifier in the small-signal procedure.

Refer to state-space Eq. (3) where the state vector $x = \begin{bmatrix} i_d\ i_q\ v_o\ \Delta v_o \end{bmatrix}^T$, the input vector $u = \begin{bmatrix} v_d\ v_q \end{bmatrix}^T$,

$$\text{The state matrix } A = \begin{bmatrix} G_{id11}(s) & G_{id12}(s) & G_{id13}(s) \\ G_{id21}(s) & G_{id22}(s) & G_{id23}(s) \\ G_{vd11}(s) & G_{vd12}(s) & G_{vd13}(s) \\ G_{\Delta vd11}(s) & G_{\Delta vd12}(s) & G_{\Delta vd13}(s) \end{bmatrix},$$

$$\text{The input matrix } B = \begin{bmatrix} G_{iv11}(s) & G_{iv12}(s) \\ G_{iv21}(s) & G_{iv22}(s) \\ G_{vv11}(s) & G_{vv12}(s) \\ G_{\Delta vv11}(s) & G_{\Delta vv12}(s) \end{bmatrix}$$

$$\frac{d}{dt}\begin{bmatrix} i_d \\ i_q \\ v_o \end{bmatrix} = \begin{bmatrix} G_{id11}(s) & G_{id12}(s) & G_{id13}(s) \\ G_{id21}(s) & G_{id22}(s) & G_{id23}(s) \\ G_{vd11}(s) & G_{vd12}(s) & G_{vd13}(s) \\ G_{\Delta vd11}(s) & G_{\Delta vd12}(s) & G_{\Delta vd13}(s) \end{bmatrix}\begin{bmatrix} i_d \\ i_q \\ v_o \end{bmatrix} + \begin{bmatrix} G_{iv11}(s) & G_{iv12}(s) \\ G_{iv21}(s) & G_{iv22}(s) \\ G_{vv11}(s) & G_{vv12}(s) \\ G_{\Delta vv11}(s) & G_{\Delta vv12}(s) \end{bmatrix}\begin{bmatrix} v_d \\ v_q \end{bmatrix}$$

(10)

where the symbol is in the form $G_{ab\beta\gamma}$, such as, a is output, that is, an element of vector x, b is input, that is, an element of a vector u, β is rank of the output a in the vector x, and γ is the rank of the input b in the vector u. The list of transfer functions $G_{ab\beta\gamma}$ and their parameters are given in Appendices A and B, respectively, and transfer function is shown in Figure B1 (Appendix B). The equivalent transfer function that represents the Vienna-I rectifier is given by taking Laplace transform for (10), and Figure 2 shows the transfer function representation [26].

3. DC-Bus Voltage Controller Design

As shown in Figure 3 [27] in a dq-frame, V_{DC}^2 is compared with V_{DCref}^2, the compensator $K_v(s)$ objective is to compensate the error signal e_V, and the command of active power P_s controller is done by P_{sref}, also Q_{sref} can control the reactive power Q_s. $G_v(s)$ is a factor of the primary DC capacitance and a time response to a step input signal. The DC voltage controller is designed for the worst-case design conditions of the rectification mode to regulate the DC voltage across the DC-bus. Furthermore, the following equations can define the DC voltage controller.

$$G_v\left(s\right) = -\frac{2}{C}\left(\frac{\tau s + 1}{s}\right)$$

(11)

where τ is a time constant for the controller, and C is the rectifier capacitance. The compensator gain $K_v(s)$ is shown as follows.

$$K_v\left(s\right) = N\left(s\right) \times \frac{K_0}{S}$$

(12)

where $N(s)$ is the controller transfer function, K_0 is the constant value of gain. To ensure zero steady-state error $K_v(s)$ has to include an integral term. The lead filter equation $N(s)$ in Eq. (12) can be written as shown in Eq. (13) to obtain a stable closed-loop system for operating points,

$$N\left(s\right) = n_0\left(\frac{(s + (p/\alpha))}{(s + p)}\right)$$

(13)

where n_0 is the filter gain, p is a filter pole, and α (> 1) is a fixed and real value.

Figure 3. Block diagram of a DC-bus voltage controller [27].

The value of the filter phase δ_m is given by

$$\delta_m = \arcsin\left(\frac{\alpha - 1}{\alpha + 1}\right)$$

(14)

The compensator frequency ω_m is shown as

$$\omega_m = \frac{p}{\sqrt{\alpha}}$$

(15)

Then, the compensator gain $K_v(s)$ in the closed-loop transfer function can be obtained as

$$K_v\left(s\right) = \frac{200s + 14000}{s^2 + 2274s}\,(16)$$

Figure 4 shows that the system is unstable when operating in an uncompensated mode of operation. The values of parameters used are shown in Table 1.
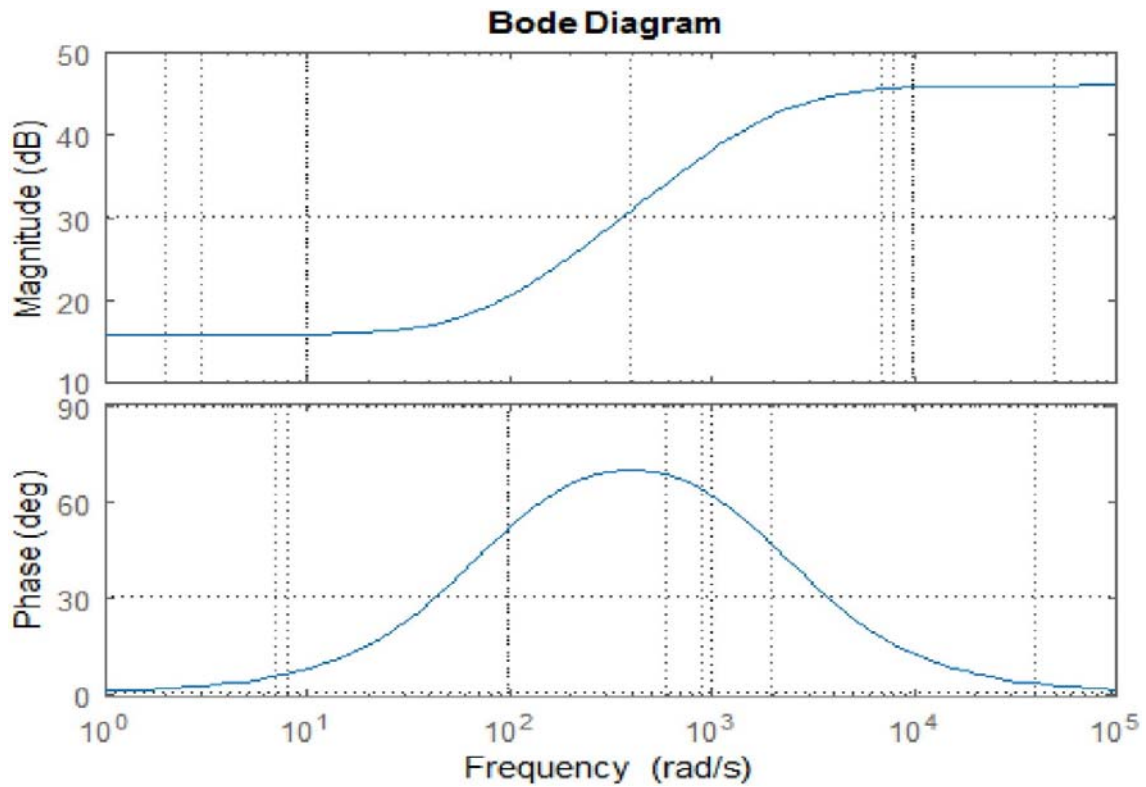
Figure 4. Bode plots of the uncompensated loop gain.

TABLE 1. Parameters used for bode plots.

Quantity	Comment	Value
δ_m	Maximum phase of the filter	$70°$
ω_m	Compensator frequency	400 rad/s
n_0	Filter gain	2
k_0	Constant gain	100

The transfer function of the compensated loop gain is given as follows,

$$L(s) = -K_v(s)G_p(s)G_v(s)$$

(17)

where $G_p(s)$ is the closed-loop transfer function.

$$G_p\left(s\right) = \frac{1}{\tau_i s + 1} = \frac{1/\tau}{s + 1/\tau}$$

(18)

From Eqs. (14) and (15), respectively, $\alpha = 32.3$, and $p = 2274$. Then, the transfer function of the overall voltage-loop gain can be deduced from Eq. (17) as follows,

$$L\left(s\right) = \frac{200*10^6 s + 200*10^3}{1000s^3 + 1000*10^3 s^2}$$

(19)

Bode plots of the overall voltage-loop gain transfer function are given in Figure 5.
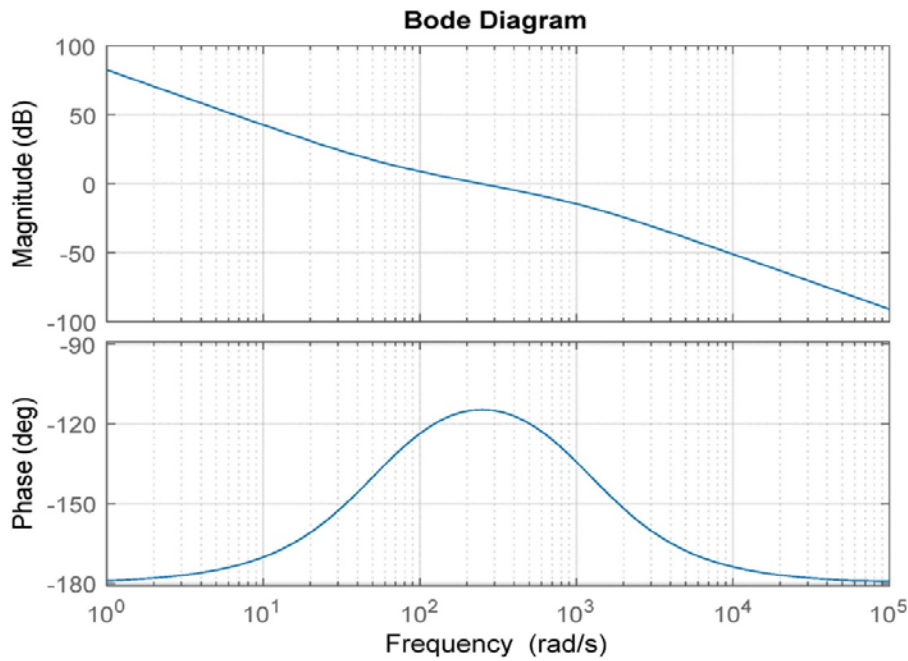
Figure 5. Bode plots of the overall voltage loop gain.

The frequency response sketched in Figure 5 shows that the closed-loop system is stable with the phase margin of $63°$ and the gain margin of 70 dB.

4. Fault Effect Elimination and Analysis

The simulated WPP consists of three parallel-connected WECUs supplying a DC load with the cost of 400 USD; for building a system consisting of 54 diodes, nine IGBT switches, three AC power supplies, and DC load resistor, inductor and capacitor. The values used in simulations are shown in Table 2.

TABLE 2. Parameters used for simulation.

Parameter	Description	Value
E	Rated voltage of the PMSG	400 V
R	Generator resistance	$1\,\Omega$
L	Generator inductance	$2\,mH$
I	Generator rated current	$40\,A$
f	Generator frequency	$60\,Hz$
Co	Rectifier output capacitor	$2000\,\mu F$
RL	Load	$50\,\Omega,\ 0.01\,mH$

An AC fault is applied to unit 2 terminals; this type of fault is due to unbalance between phases and is called an unsymmetrical shunt fault. A shunt fault is defined as "an unbalance between phases or between phase and ground." A series fault is defined as "an unbalance in the same line impedances."

Shunt faults are an essential class of faults and include various types of short circuits as well as unbalanced loads, and can be summarized as follows,

1. Line to ground faults.

2. Line to line faults.

3. Double line to ground faults.

4. Triple line to ground faults [28, 29].

In this article generator line to ground and double line to ground, faults have been discussed. Figure 6 explains the simulated system.

If the fault current exceeds the thermal capability of the Vienna rectifier-I valves, the IGBT switch will be blocked, and the system will stop operating until the fault is cleared. In such a case, the system needs to be restarted.
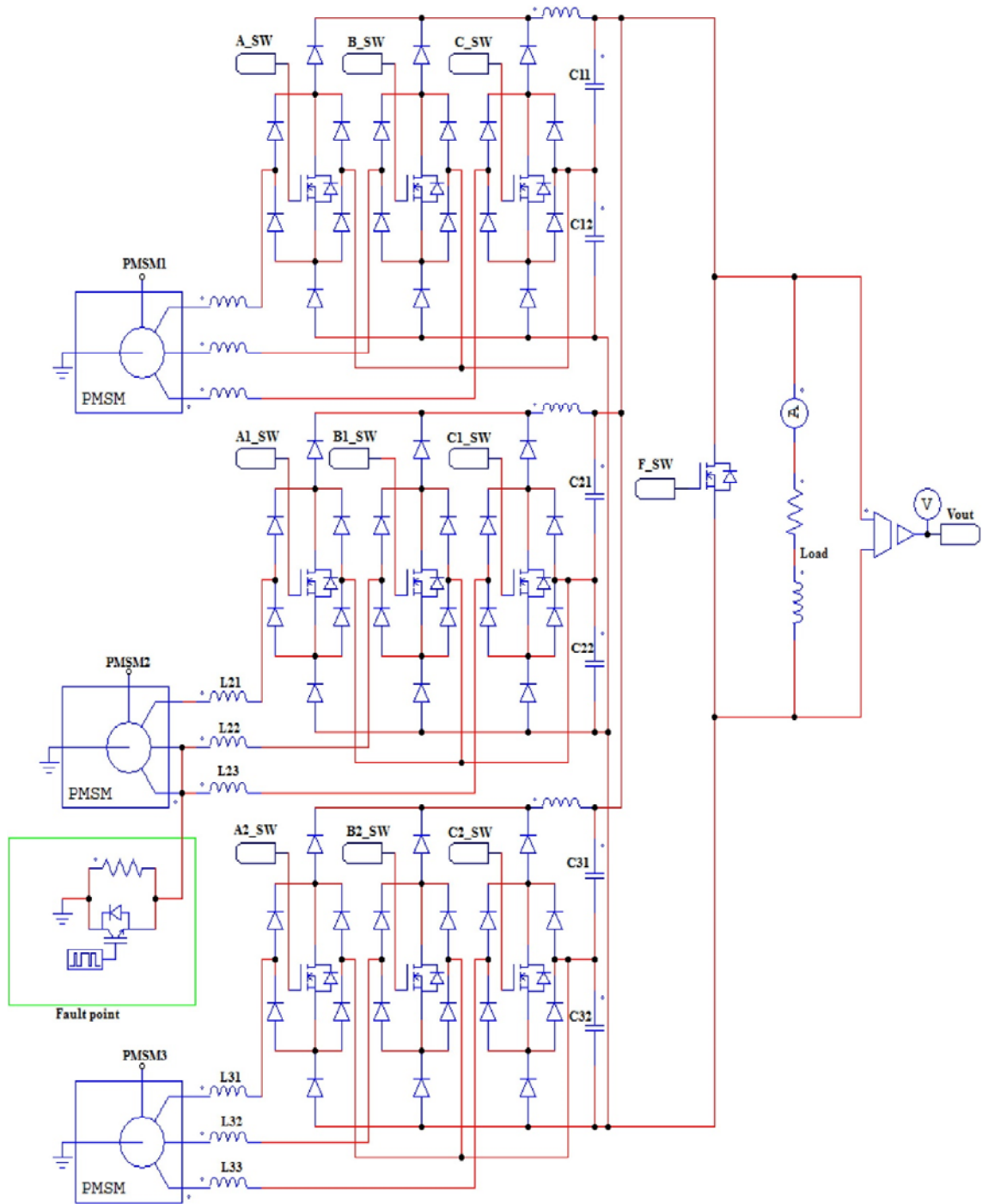
Figure 6. The simulated system considering the fault in generator 2.

Figure 7 shows the FRT controller. The rectifier output voltage V_{out} (t) is sensed with the sensor gain H(s), the sensor output will be H(s)*V_{out} (s) which is compared with a reference input voltage V_{ref} (s). In case of disturbances or component variations in the compensator the difference in the V_{ref} "the input voltage reference" and H(s)*V_{out} (s) "the sensor output" is named an error signal. The aim is to let H(s)*V_{out} (s) equal to V_{ref} (s) to obtain zero error, but practically, the error signal is a commonly small value. The output of the controller is the gate triggering circuit (F_sw) shown in Figure 6. The proposed sub-module (SM) control circuit has been constructed to reduce the fault effect. The recent grid codes require that AC generator-based variable speed WPP should be held in operation during fault cases. The Simulink representation for the controller is shown in Figure 8.
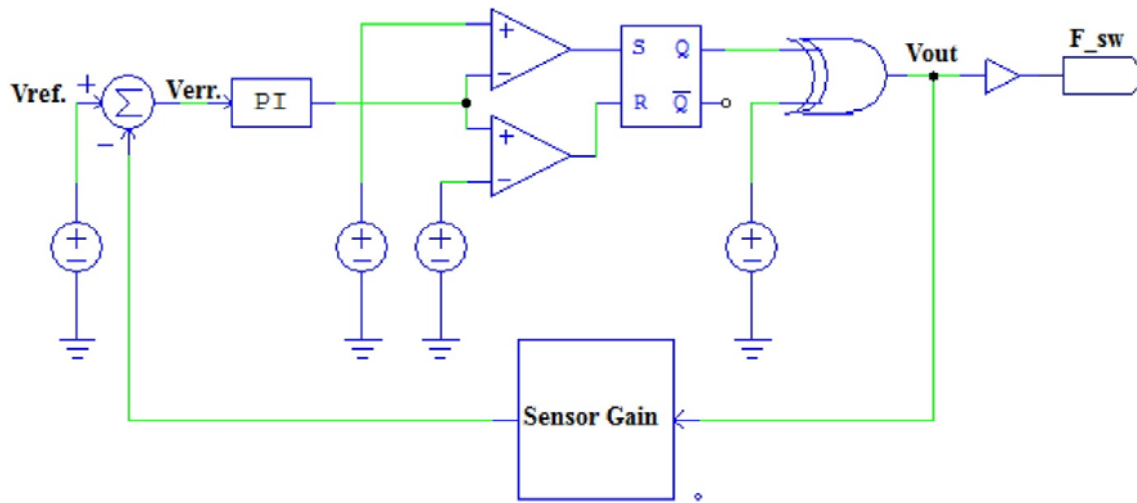
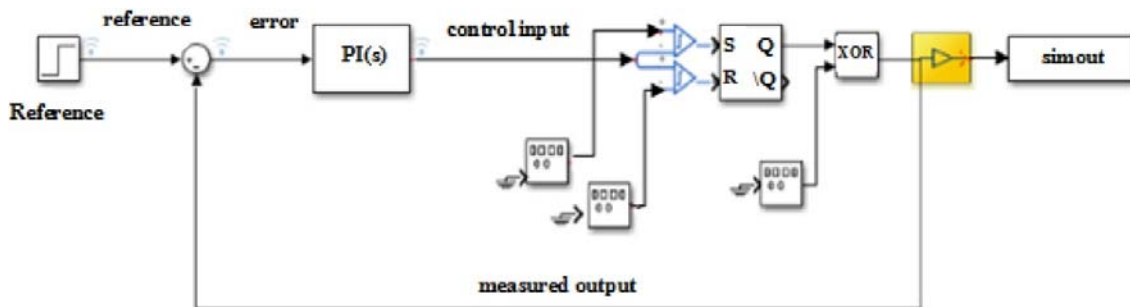**Figure 7**. Schematic diagram of the FRT controller.

Figure 8. Simulink representation of the FRT controller.

## 5. Simulation Results and Discussion

Simulations have been built on the PSim program. Three WECUs are constructed in parallel, so that the parallel connection is the most reliable type of connection, that if one unit collapses the system remains in synchronism. Several modes of operation have been simulated and are presented as follows.

5.1. Steady-state operation

In a steady-state operation, the switch will be locked for a long time, so the voltage and current waves are in stable performance. Figure 9 shows the generator AC output voltage it is 390 V and the current is 38 A. There are small transients at the beginning of both voltage and current waves, due to the starting of the generator.
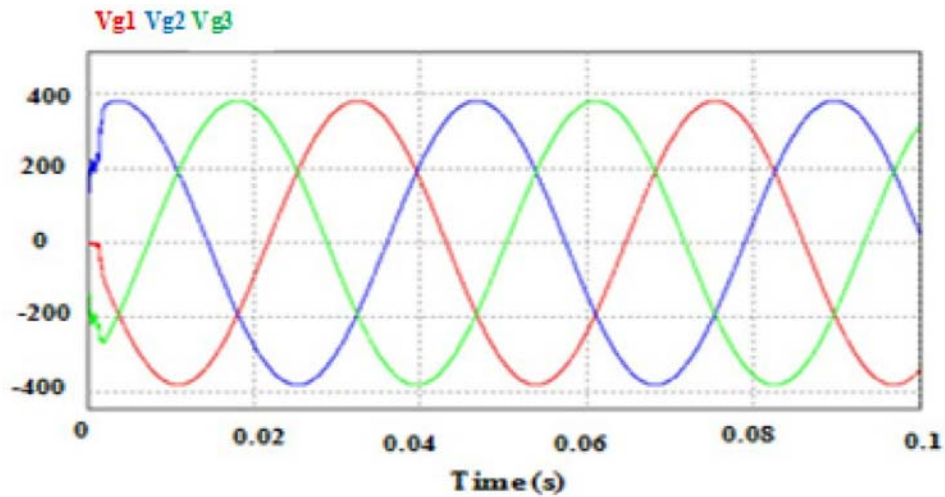

(a)
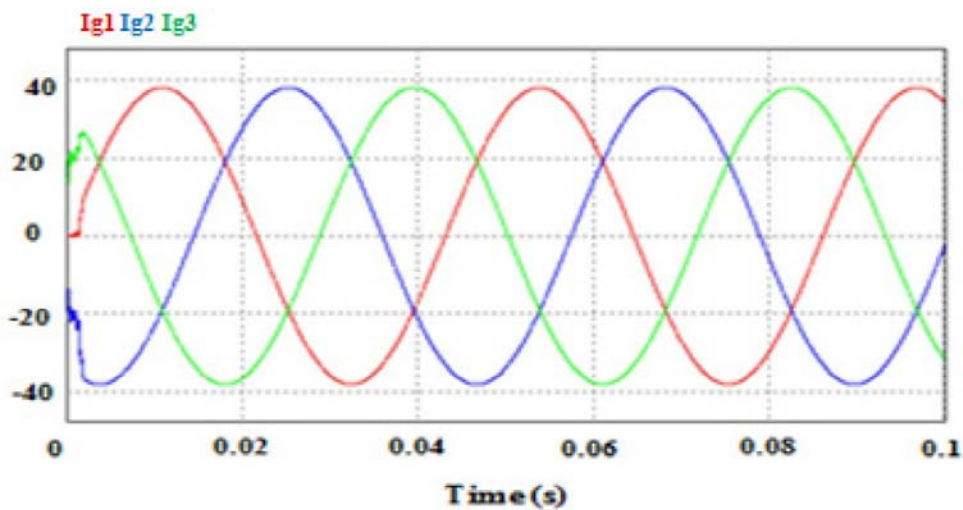
(b)

Figure 9. Generator output, (a) output voltage and (b) output current.

Figure 10(a) and (b) show the output voltage and current waveforms. The output voltage as shown is in steady-state condition and is stable at 400 V after small overshooting to 510 V due to system startup. The same as output voltage the output current as shown is in regular performance and stable at 40 A after some overshooting up to 52 A.
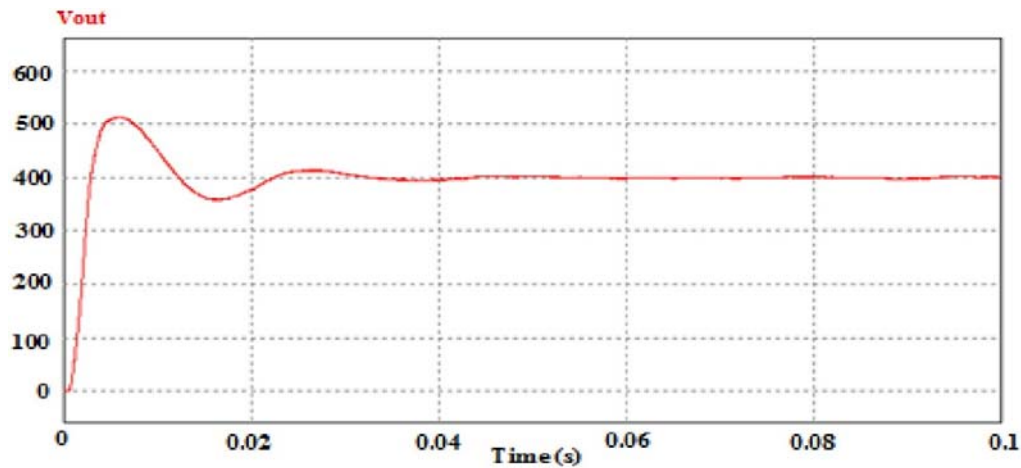
(a)
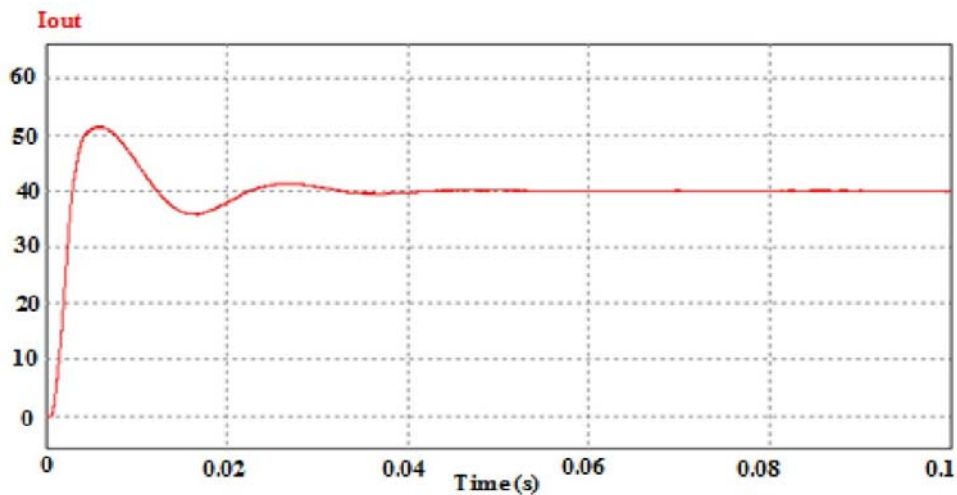
(b)

Figure 10. Steady-state components, (a) output voltage and (b) output current.

The positive points of these waveforms are (i) less transient time; 0.03 s for voltage and current waveforms, (ii) the under and overshooting are running in a short time and one cycle; in 0.025 s 152 V overshooting and 50 V undershooting, 12 A overshooting and 5 A undershooting, and (iii) no ripple disturbance in the voltage and current waves.

5.2. Unsymmetrical fault simulation

5.2.1. Line to ground fault

When the line-to-ground fault occurs, then still the output parameters are same as steady-state parameters because of parallel connection of units; if the unit collapsed the system will remain in synchronism.

Figure 11(a) and (b) show the output waveforms. Figure 11(a), shows the output voltage; which is identical to the steady-state value, and stable at 400 V after over and undershooting in one cycle up around 102 V or 25.5% from the original voltage value, and down to around 50 V or 12.5% from the original voltage value. Also, the output current in Figure 11(b) is stable and constant at 40 A after small overshooting (due to switching) up to 11 A or 27.5% from the original current value, and undershooting down to 5 A or 12.5% from the original current value. The transients in voltage and current waves are continuing for a very few times approximately 0.025 s.
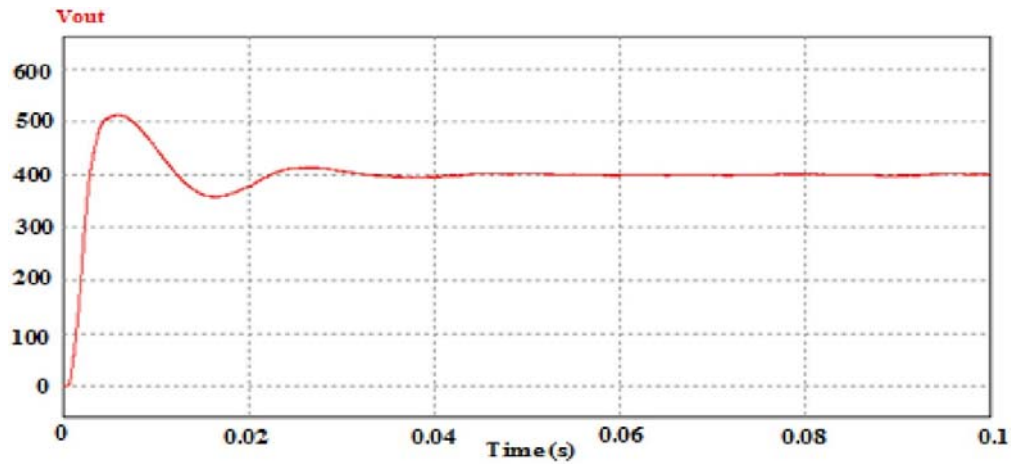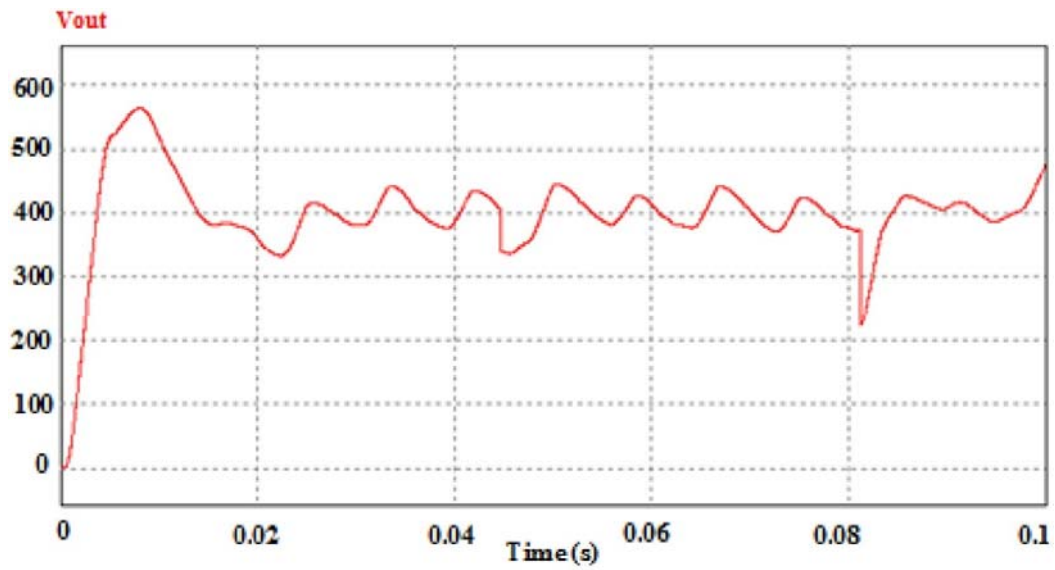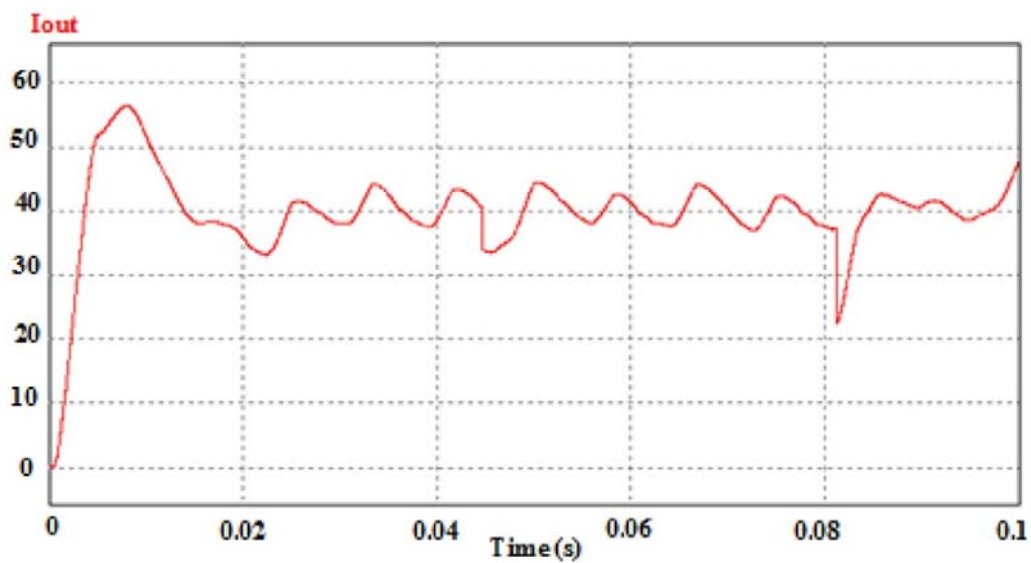

(a)
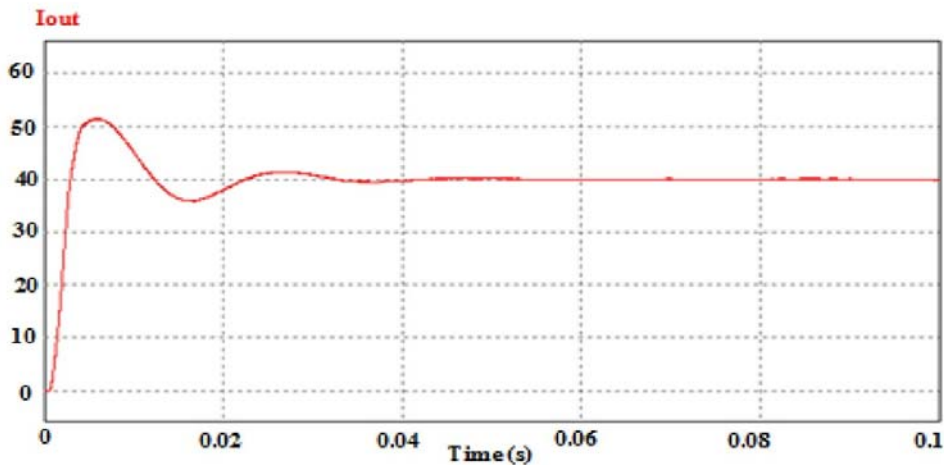
(b)

Figure 11. DC components when applying a line to ground fault, (a) output voltage and (b) output current.

5.2.2. Double line to ground fault

When applying double lines to ground fault as shown in Figure 12(a) and (b), the output voltage and current waves are fluctuated (current is fluctuating through the load) due to the fault.

16

(a)

(b)

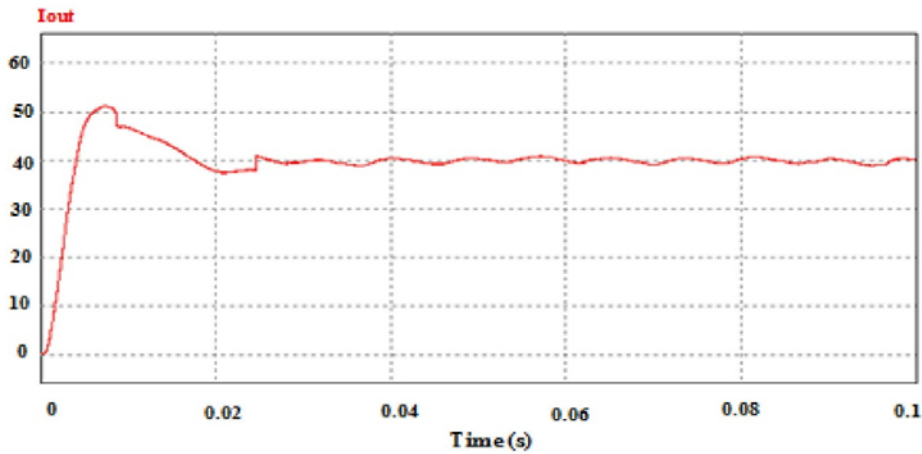**Figure 12.** Components when applying two lines to ground fault, output voltage and (b) output current.

The output voltage as shown in Figure 12(a) is fluctuating around 400 V, with small overshooting up to about 560 V and shooting down to about 215 V. The output current wave as indicated in Figure 12(b), is fluctuating through 40 A after overshooting up to about 56 A and shooting down to about 21 A.

5.3. FRT controller

Figure 13 shows a fault controller waveform in two lines to ground fluctuation fault, to enhance the system stability and reliability; by allowing the path of current from capacitors through the diodes and the rectifier to the load. Nevertheless, if the switch is opened, the diode will become forward-biased relative to the capacitors.
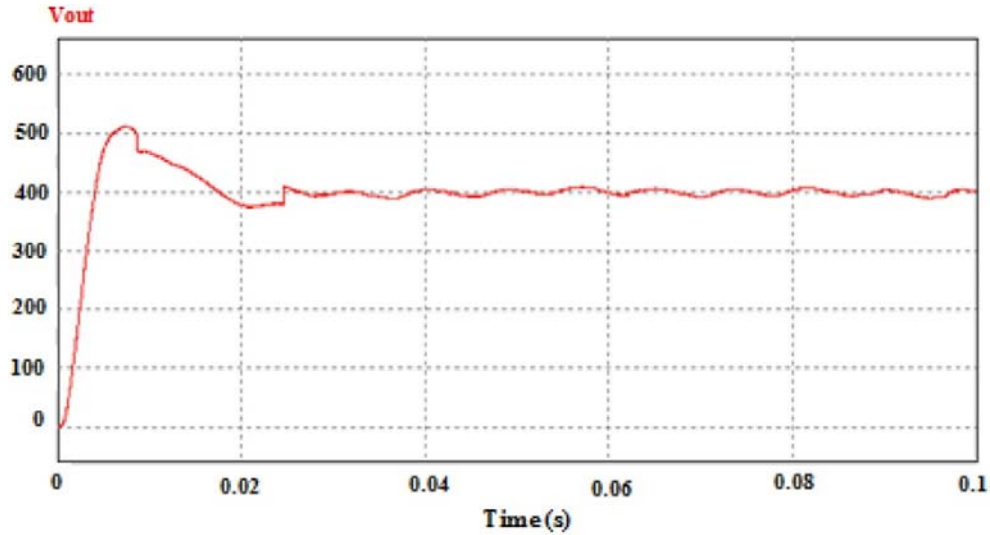
(a)

(b)

Figure 13. Components when applying extra circuit for ride-through two lines to ground fault, (a) output voltage and (b) output current.

The voltage and current magnitudes are around 400 V and 40 A, with accepted voltage and current ripple percentage; around 1.3% for both. There is overshooting in a voltage wave around 110 V or 27.5% of the original voltage value due to switching, continuing for only one cycle, and shooting down 20 V or 5% of the original voltage value, moreover, for the current wave there is shooting up about 12 A or 30% of the original

current value, and shooting down 3 A or 7.5% of the original current value.

Vsw in Figure 14 is a switching voltage, and Vout is a DC output voltage. The standard voltage is 400 V, and the acceptance error is around ± 10%, so it is from 440 V up and 360 V down. The fault time started when the voltage was fluctuating from 300 to 490 V at 0.06 s, and the fault clearance time should be after 120 ms.
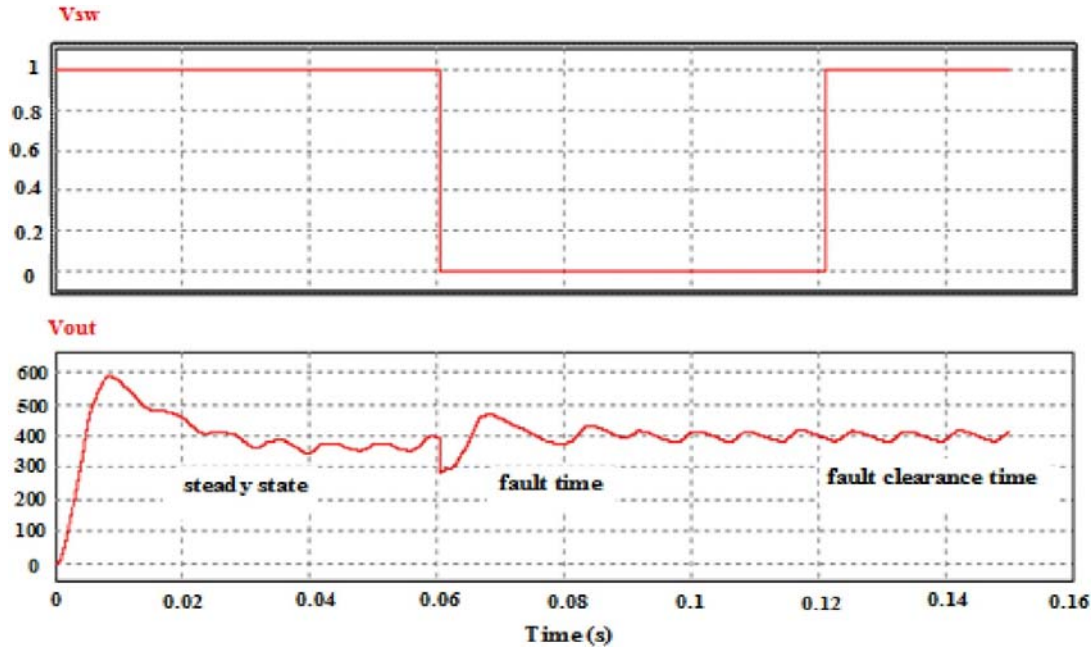
Figure 14. Switching and output voltages; to clarify the fault time.

The operation under unsymmetrical fault creates unbalanced currents between the generator phases and torque pulsation as shown in Figure 15. If this situation is continued for long-term, the unbalanced currents might produce heating in the three phases, which affects the insulation of windings, as well as operation under symmetrical fault, turning to high short circuit currents at the fault location [28].

Figure 15. Generator output currents while the double line to ground fault occurs.

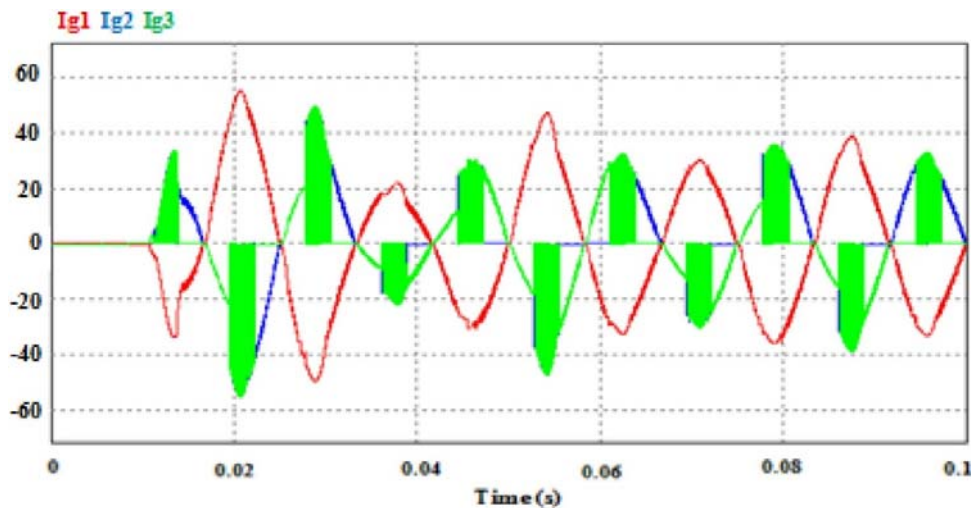## 6. Conclusion

This article has presented a FRT controller, by utilizing the proposed proportional-integral (PI) and electronic sensors; considering the economical operation. The suggested SM eliminates the fault current effect by controlling the output voltage. Several modes of operation have been discussed. The simulation results confirm the reliability of the proposed FRT module. Fault currents can be blocked rapidly to protect power tools from overheating problems. In conclusion, it has been found that the WTG integrated with a Vienna-I based DC transmission system is a practical candidate that can be employed in large-scale WPPs to realize a stable and reliable operation.

Notes on contributors

Inas Mohammed Osman Mohammed has received her Ph.D. in the department of electrical, electronic and computer engineering at University of Pretoria, South Africa in 2021. She received her B.Sc. and M.Sc. degrees in electrical power engineering from University of Red Sea, Sudan, and University of Khartoum, Sudan, in 2005 and 2013 respectively. From June 2005 to date she is working as electrical engineer for ministry of physical plan and public utilities, Sudan. From February 2008 to January 2012 she worked as a Teaching Assistance at University of Red Sea - Faculty of Engineering, Sudan. Her research interests include renewable energy, power electronics applications in renewable energy systems.

Michael Njoroge Gitau is currently a Professor in the Department of Electrical, Electronics and Computer Engineering at University of Pretoria in South Africa. He has more than 30 years of industrial, teaching and research experience. His research interests are in converter modelling, conducted EMI and integration of renewable energy sources into the grid.

Ramesh Bansal has more than 25 years of teaching, research, academic leadership, and industrial experience. Currently, he is a Professor in EE Department, University of Sharjah (UAE). In previous postings, he was Professor and Group head (Power) in EEC Department, University of Pretoria (South Africa) and worked with the University of Queensland (Australia); University of the South Pacific (Fiji); BITS Pilani (India); and Civil Construction Wing, All India Radio. Prof. Bansal has published over 400 journal articles, conference papers, books, books chapters. He has Google s of 15000 and h-index 58. He has supervised 25 PhD and 5 Post Docs. He is an Editor/AE of IET-RPG, Tech. Eco. Smart Grids and Sust. Energy, and Electric Power Comp. and Systems. He is a Fellow, and CP Engg IET-UK, Fellow Institution of Engineers (India). His research interests include renewable energy, power systems, and smart grid.

References

1. S. S. Sahoo, A. Roy and K. Chatterjee, "Fault ride-through enhancement of wind energy conversion system adopting a mechanical controller," presented at National Power Systems Conference (NPSC), Bhubaneswar, India, 2016. pp. 1–5.
2. M. O. Mohammed, M. N. Gitau, R. C. Bansal and K. Musasa, "Modelling and control of a Vienna smart rectifier-I for wind power systems integrated under transient conditions," *Technol. Econ. Smart Grids Sustain. Energy*, vol. 4, no. 2, pp. 1–13, 2019. DOI: 10.1007/s40866-018-0057-6.
3. L. Gidwani, H. Tiwari and R. C. Bansal, "Improving power quality of wind energy conversion system with unconventional power electronic interface," *Int. J. Elect. Power Energy Systems*, vol. 44, no. 1, pp. 445–453, 2013. DOI: 10.1016/j.ijepes.2012.07.051

4. S. Wang, *et al.*, "Flexible fault ride through strategy for wind farm clusters in power systems with high wind power penetration," *Energy Convers. Manage.*, vol. 93, pp. 239–248, 2015. DOI: 10.1016/j.enconman.2015.01.022.

5. K. Musasa, N. I. Nwulu, M. N. Gitau and R. C. Bansal, "A review on DC collection grids for offshore wind farms with HVDC transmission system," *IET-Power Electronics*, vol. 10, no. 15, pp. 2104–2115, 2017. DOI: 10.1049/iet-pel.2017.0182.

6. K. Musasa, M. N. Gitau and R. C. Bansal, "Dynamic analysis of DC-DC converter internal to an offshore wind farm," *IET-Renew. Power Gen.*, vol. 9, no. 6, pp. 542–548, 2015. DOI: 10.1049/iet-rpg.2014.0420.

7. V. Gevorgian, Y. Zhang and E. Ela, "Investigating the impacts of wind generation participation in interconnection frequency response," *IEEE Trans. Sustain. Energy*, vol. 6, no. 3, pp. 1004–1012, 2015. DOI: 10.1109/TSTE.2014.2343836.

8. R. C. Bansal, "Three-phase self-excited induction generators (SEIG): An overview," *IEEE Trans. Energy Convers.*, vol. 20, no. 2, pp. 292–299, 2005. DOI: 10.1109/TEC.2004.842395.

9. S. Swain and P. K. Ray, "Short circuit fault analysis in a grid connected DFIG based wind energy system with active crowbar protection circuit for ridethrough capability and power quality improvement," *Int J. Elect. Power Energy Syst.*, vol. 84, pp. 64–75, 2017. DOI: 10.1016/j.ijepes.2016.05.006.

10. R. C. Bansal, T. S. Bhatti and D. P. Kothari, "Some aspects of grid connected wind electric energy conversion systems," *Interdiscipl. J. Inst. Eng. (India)*, vol. 82, no. 1, pp. 25–28, 2001.

11. L. Chen, Y. Dai, Y. Min and K. Hou, "Study on the mechanism of transient voltage stability of wind power with power electronic interface," presented at Asia-Pacific Power and Energy Engineering Conference, Brisbane, Australia, 2015. pp 1–5.

12. J. Tan and Y. Zhang, "Coordinated control strategy of a battery energy storage system to support a wind power plant providing multi-timescale frequency ancillary services," *IEEE Trans. Sustain. Energy*, vol. 8, no. 3, pp. 1140–1153, 2017. DOI: 10.1109/TSTE.2017.2663334.

13. R. C. Bansal, T. S. Bhatti and V. Kumar, "Reactive power control of autonomous wind-diesel hybrid power systems using ANN," presented at Proc. 8th Int. Power Engineering Conf. (IPEC 2007), Singapore, 2007. pp. 1376–1381.

14. S. K. Chaudhary, R. Teodorescu, P. Rodriguez and P. C. Kjaer, "Chopper controlled resistors in VSC-HVDC transmission for WPP with full-scale converters," presented at IEEE Sustainable Alternative Energy (SAE) Conf, Valencia, Spain, 2009. pp. 1–8.

15. M. Tazil, et al., "Three-Phase doubly-fed induction generators: an overview," *IET Electr. Power Appl.*, vol. 4, no. 2, pp. 75–89, 2010. DOI: 10.1049/iet-epa.2009.0071.

16. S. D. Round, P. Karutz, M. L. Heldwein and J. W. Kolar, "Towards a 30 kW/liter, three- phase unity power factor rectifier," presented at Power Conversion Conf, Nagoya, Japan, 2007. pp. 1251–1259.

17. J. Adhikari, I. V. Prasanna and S. K. Panda, "Voltage oriented control of the three-level vienna rectifier using vector control method," presented at Applied Power Electronics Conf. and Exposition (APEC), Long Beach, USA, 2016. pp. 9–16.

18. J. Monroy-Morales, M. ez-Angeles, D. Campos-Gaona, R. Pena-Alzola, M. Ordonez and W. Merida, "Modeling and control design of a vienna rectifier based electrolyzer," presented at 7th International Symposium on Power Electronics for Distributed Generation Systems (PEDG), Vancouver, Canada, 2016. pp. 1–8.

19. V. Yaramasu and B. Wu, "Predictive control of a three-level boost converter and an NPC inverter for high-power pmsg-based medium voltage wind energy conversion systems," *IEEE Trans. Power Electron*, vol. 29, no. 10, pp. 5308–5322, 2014. DOI: 10.1109/TPEL.2013.2292068.

20. Rajaei, M. Mohamadian and A. Y. Varjani, "Vienna-rectifier-based direct torque control of PMSG for wind energy application," *IEEE Trans. Ind. Electron*, vol. 60, no. 7, pp. 2919–2929, 2013. DOI: 10.1109/TIE.2012.2227905.
21. T. Gao, S. Zhang, S. Zhang and J. Zhao, "A dynamic model and modified one-cycle control of three- level front-end rectifier for neutral point voltage balance," *IEEE Access*, vol. 5, pp. 2000–2010, 2017. DOI: 10.1109/ACCESS.2017.2668398.
22. T. Thangavelu, P. Shanmugam and K. Raj, "Modelling and control of VIENNA rectifier a single phase approach," *IET Power Electronics*, vol. 8, no. 12, pp. 2471–2482, 2015. DOI: 10.1049/iet-pel.2014.0503.
23. H. M. Teshnizi, A. Moallem, M. R. Zolghadri and M. Ferdowsi, "A dual-frame hybrid vector control of vector-modulated VIENNA I rectifier for unity power factor operation under unbalanced mains condition," presented at Applied Power Electronics Conf. and Exposition, Austin, USA, 2008. pp. 1402–1408.
24. L. Hang, H. Zhang, S. Liu, X. Xie, C. Zhao and S. Liu, "A novel control strategy based on natural frame for Vienna-Type rectifier under light unbalanced-grid conditions," *IEEE Trans. Ind. Electron*, vol. 62, no. 3, pp. 1353–1362, 2015. DOI: 10.1109/TIE.2014.2364792.
25. S. Howell, S. Filizadeh and A. M. Gole, "Unidirectional HVDC topology with DC fault ride-through capability," *Can. J. Electr. Comput. Eng.*, vol. 40, no. 1, pp. 41–49, 2017. DOI: 10.1109/CJECE.2016.2629460.
26. N. Youssef, K. Al-Haddad and H. Kanaan, "Implementation of a new linear control technique based on experimentally validated small-signal model of three-phase three-level boost-type vienna rectifier," *IEEE Trans. Ind. Electron*, vol. 55, no. 4, pp. 1666–1676, 2008. DOI: 10.1109/TIE.2008.918622.
27. Yazadani and R. Iravani, *Voltage-Sourced Converters in Power Systems: Modelling, Control and Applications*. Hoboken, New Jersey and Canada: John Wiley Sons Inc., 2010.
28. P. M. Anderson, *Analysis of Faulted Power Systems*. New York, USA: IEEE Press, 1995.
29. M. Stemmle, *et al.*, "Analsis of unsymmetrical faults in high voltage power systems with superconducting fault current limiters," *IEEE Trans. Appl. Supercond.*, vol. 17, no. 2, pp. 2347–2350, 2007. DOI: 10.1109/TASC.2007.899136.

Appendix A

The transfer-functions $G_{ab\beta\gamma}$

$$G_{id11}\left(s\right) = -\frac{V_o^*}{2L}\frac{\left(S^2 + \delta_{11}S\right)}{den(s)}$$

(A.1)

where

$$den\left(s\right) = S^3 + \tau_0 S^2 + \left(\omega_0^2\delta_{12} + \delta_{13}\right)S + \tau_0\omega_0^2$$

(A.2)

$$G_{id12}\left(s\right) = -\frac{V_o^*\omega_0}{2L}\frac{\left(S + \delta_{11}\right)}{den(s)}$$

(A.3)

$$G_{id13}\left(s\right) = 0$$

(23)

$$G_{id21}\left(s\right) = -\frac{V_o^*\omega_0}{2L}\frac{\left(\delta_{11}S + \tau_0\right)}{den(s)}$$

(A.4)

$$G_{id22}\left(s\right) = -\frac{V_o^*}{2L}\frac{\left(S^2 + \tau_o S + \delta_{13}\right)}{den(s)}$$

(A.5)

$$G_{id23}\left(s\right) = 0$$

(A.6)

$$G_{iv11}\left(s\right) = \frac{\left(S^2 + \tau_o S + \delta_{16}\right)}{L \times den(s)}$$

(A.7)

$$G_{iv12}\left(s\right) = \frac{\omega_0}{L}\frac{\left(S^2 + \delta_{11}\right)}{den(s)}$$

(A.8)

$$G_{iv21}\left(s\right) = -\frac{\omega_0}{L}\frac{\left(S^2 + \delta_{17}\right)}{den(s)}$$

(A.9)

$$G_{iv22}\left(s\right) = \frac{\left(S^2 + \tau_0 S + \delta_{13}\right)}{L \times den(s)}$$

(A.10)

$$G_{vd11}\left(s\right) = \frac{3\sqrt{2} \times I_s^*}{2 \times C_0} \frac{\left(S^2 + \delta_{14}S\right)}{den(s)}$$

(A.11)

$$G_{vd12}\left(s\right) = \frac{3\sqrt{2} \times I_s^* \times \omega_0}{2 \times C_0} \frac{\left(S^2 + \delta_{14}\right)}{den(s)}$$

(A.12)

$$G_{vd13}(s) = 0$$

(A.13)

$$G_{\Delta vd11}(s) = 0$$

(A.14)

$$G_{\Delta vd12}(s) = 0$$

(A.15)

$$G_{\Delta vd13}\left(s\right) = \frac{\delta_{11}\sqrt{2} \times I_s^*}{C_0 \times (S + \delta_{15})}$$

(A.16)

$$G_{vv11}\left(s\right) = \frac{3\sqrt{2} \times V_s}{L \times C_0 \times V_0^*} \times \frac{S + \delta_{18}}{den(s)}$$

(A.17)

$$G_{vv12}\left(s\right) = -\frac{3\sqrt{2} \times I_S^* \times \omega_0}{C_0 \times V_0^*} \times \frac{(S - \delta_{14})}{den(s)}$$

(A.18)

$$G_{\Delta vv11}(s) = 0$$

(A.19)

$$G_{\Delta vv12}(s) = 0$$

(A.20)

Appendix B

Transfer-function parameters

$$\tau_0 = \frac{1}{C_o R_o} = \frac{1}{2000 \times 10 - 6 \times 50} = 10$$

(B.1)

$$\delta_{11} = \tau_0 + \frac{6V_s \times I_s^*}{C_o \times V_o^{*2}} = 310$$

(B.2)

$$\delta_{12} = 1 + \frac{6L \times I_s^{*2}}{C_o \times V_o^{*2}} = 1.06$$

(B.3)

$$\delta_{13} = \frac{6V_s^2}{LC_o V_o^{*2}} = 1.5 \times 10^6$$

(B.4)

$$\delta_{14} = -\frac{V_s}{LI_s^*} = -0.2 \times 10^6$$

(B.5)

$$\delta_{15} \cong 2\tau_0 = 20$$

(B.6)

$$\delta_{16} = \frac{6 \times L \times \omega_0^2 \times I_s^{*2}}{C_o \times V_o^{*2}} = 8527.3$$

(B.7)

$$\delta_{17} = \tau_0 + \frac{6 \times V_s \times I_s^{*2}}{C_o \times V_o^{*2}} = 12010$$

(B.8)

$$\delta_{18} = L\omega_0^2 I_s^* = 79.6 \times 10^6$$

(B.9)

$$den(s) = S^3 + \tau_0 S^2 + \left(\omega_0^2 \delta_{12} + \delta_{13}\right)S + \tau_0 \omega_0^2 = S^3 + 10S^2 + \left(1.65 \times 10^6\right)S + \left(1.4 \times 10^6\right)$$
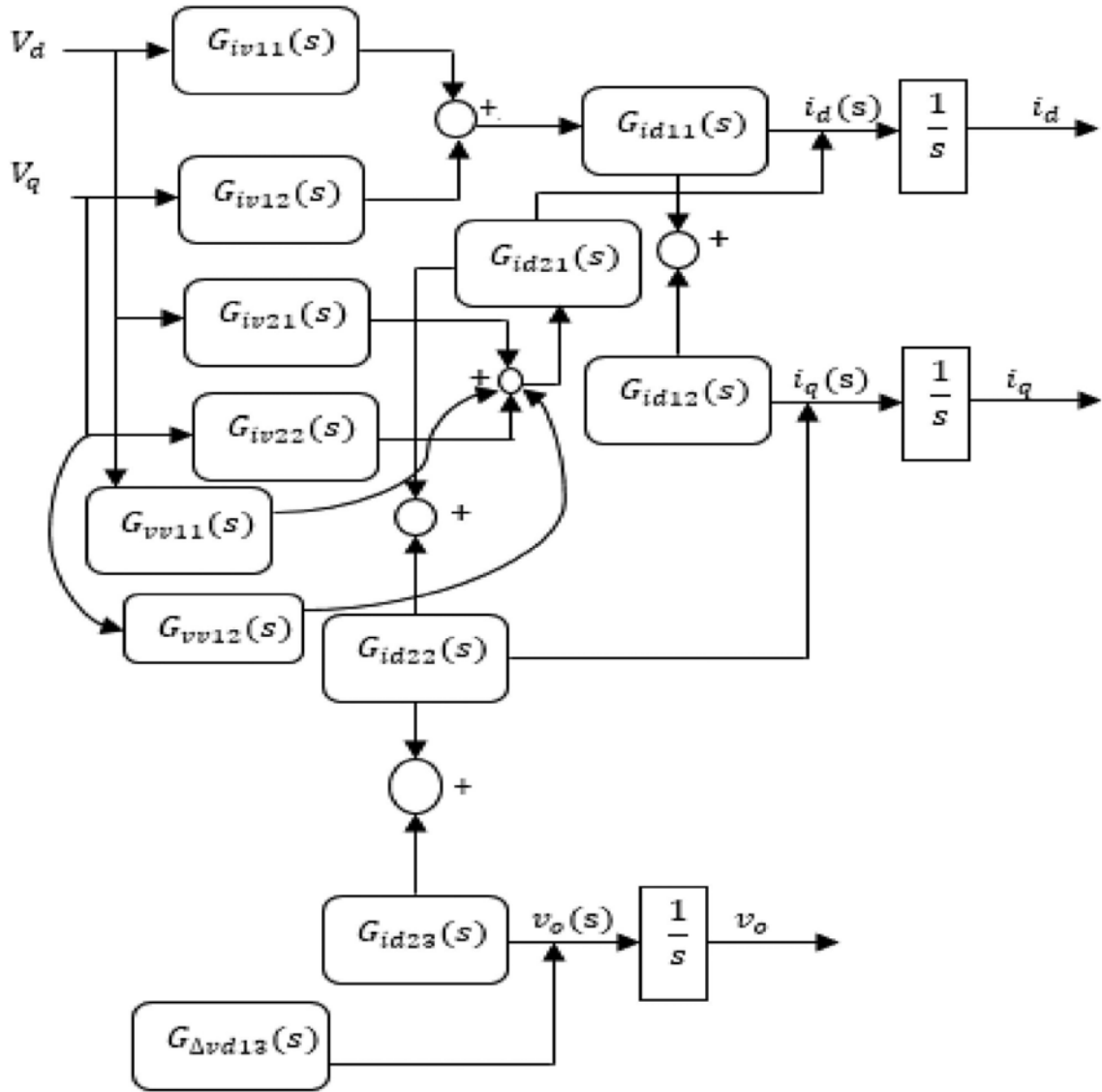
(B.10)

Figure B1. Transfer-function block diagram of the proposed rectifier in small-signal procedure.